Scripta Materialia 169 (2019) 33–37

Contents lists available at ScienceDirect

Scripta Materialia

journal homepage: www.elsevier.com/locate/scriptamat

High (10^{-3} s^{-1}) densification rates at <0.25 homologous temperature in pressure assisted densification of nanocrystalline MgO: Effects of water absorption and grain size

D.M. Dewitt, Y. Kodera, J.E. Garay *

Advanced Materials Processing and Synthesis Lab, Materials Science and Engineering Program, Mechanical and Aerospace Engineering Department, University of California, San Diego, United States of America

ARTICLE INFO

Article history:
Received 23 February 2018
Received in revised form 20 December 2018
Accepted 6 January 2019
Available online 14 May 2019

Keywords:
MgO
Water absorption
Spark plasma sintering (SPS)
Current-activated pressure-assisted densification (CAPAD)
Cold sintering

ABSTRACT

We measured the real-time densification rates in the current activated pressure assisted densification (CAPAD) of nanocrystalline MgO. The rates of samples densified from powders with grain sizes ~40 nm are similar to those measured previously for other nanocrystalline materials while those from 29 nm powder are higher. Exposing the powders to a humid environment increases the densification rates and allows densification at lower temperatures. The densification rate curves of samples with absorbed water display two peaks implying two controlling mechanisms, while the dry samples display one. We attribute lower temperature densification to $Mg(OH)_2$-MgO conversion and the higher to diffusion-controlled densification.

MgO is a useful engineering ceramic that has high temperature structural applications as well as interesting optical applications [1–4]. Consequently, the fabrication of MgO has been extensively studied by pressure-less sintering, hot pressing (HP) and current-activated pressure-assisted densification, CAPAD (often called spark plasma sintering (SPS)). Because of MgO's high temperature stability, pressure-less sintering typically requires high temperatures (>1300 °C) and long durations (>1 h.) for full density, leading to substantial grain growth (>1 μm). Well known HP experiments and models show that using nanocrystalline (nc) powders and application of pressure can dramatically increase densification rates. For example, the effect of pressure, σ and grain size, d on diffusion-controlled densification rates, $\dot{\rho}$ can be described using relations of the form [5,6]:

$$\dot{\rho} = C\left[\frac{D_i}{kT}\right][f(\rho)]\left[\frac{1}{d^m}\right]\sigma^n \quad (1)$$

where C encompasses material dependent constants, D_i is the controlling diffusion coefficient, $f(\rho)$ is a function of the instantaneous density, m is an exponent usually between 1 and 3 and n is the pressure (or stress) exponent usually between 1 and 3. Using HP, D. Ehre et al. achieved bulk relative density (RD) of 95% at 720 °C for 4 h [7] in nc-MgO. In turn, the high heating rates available in CAPAD significantly reduces the required processing time. For example, T. B. Tran et al. achieved full density at 650–800 °C using high pressure (>300 MPa) and low holding times (5–30 min) [2].

For decades researchers have recognized that the presence of water can significantly affect the sintering of MgO [8–10]. Anderson and Morgan found that water vapor enhances agglomeration and increases sintering and crystal growth rates—effects attributed to enhanced surface diffusion by adsorbed species [9]. Varela and Whittmore achieved approximately 95% of bulk density and 300 nm of grain size by pressure-less sintering at 1300 °C for 4 h in humidified argon [9].

Recently there has been interest in application of water and other liquid phases to dramatically reduce the densification temperatures in a process called cold sintering [11]. Luo and co-workers also demonstrated impressively low temperatures and short times required to densify ZnO using currents (flash sintering) of ZnO powders that had been exposed to water vapor [12]. Despite these benefits there has been little work on the role of grain size or water absorption in in-situ measured densification rates. Here we examine the effect of grain size and water vapor absorption on the densification rates of nc-MgO densified using CAPAD. Although the temperatures used here are significantly higher than those used in cold sintering, we believe that the water absorption aspects of this study are relevant to cold sintering in addition to CAPAD.

Commercially available nc-MgO powder with a nominal grain size of 50 nm (US Res. Nano.) was used. In order to obtain finer powder, commercially available $Mg(OH)_2$ powder (US Res. Nano.) with a reported 10 nm grain size was also used. All powders were calcined at 500 °C

* Corresponding author.
E-mail address: jegaray@ucsd.edu (J.E. Garay).

https://doi.org/10.1016/j.scriptamat.2019.04.020
1359-6462/

for 2 h in a box furnace and *immediately* placed under vacuum and transferred into an Ar glove box to prevent surface adsorption of water. The resulting powder from 10 nm $Mg(OH)_2$ reaction was planetary ball-milled at 300 RPM for 3 h, ground using a mortar and pestle and sieved through 325 mesh in a glove box.

DSC-TGA (TA Instruments, SDT-Q600) was performed to observe the conversion of $Mg(OH)_2$ to MgO. Fig. 1a shows DSC-TGA on the starting $Mg(OH)_2$. There is a sharp weight loss and corresponding endothermic peak starting around 300 °C, which we attribute to $Mg(OH)_2$ to MgO reaction. Although the weight loss continues until ~700 °C, most of the weight loss occurs by ~500 °C. One of the primary goals is to produce MgO with finer grains, so choosing a low temperature is crucial to minimize grain growth. To confirm that 500 °C for 2 h in a box furnace are sufficient reaction conditions, we replicated the conditions in the DSC-TGA (10 °C/min to 500 °C holding for 2 h); these results are shown Fig. 1b. The weight loss indicates negligible weight loss after 2 h hold and over 95% conversion.

0.55 g of powder was packed in a graphite die with a 9.5 mm inner diameter. The die and plunger assemblies were uniaxially pressed at 200 MPa for 5 min at room temperature prior to densification in CAPAD. The CAPAD parameters were 150 MPa, approximately 180 °C/min to 700 °C, with a 5 min. hold time at 700 °C. After CAPAD, the samples were polished and characterized. The relative density (RD) of the samples was measured using the Archimedes method and a theoretical density for MgO of 3.58 g/cm^3. Average grain size (AGS) was measured using Zeiss Sigma 500 scanning electron microscope (SEM) using a 5 kV accelerating voltage. Fracture surfaces were used for bulk samples and measurements were taken from multiple SEM micrographs from different sample regions. We consider these AGS values a conservative estimate, since only grains that could be clearly identified within SEM resolution were counted.

Fig. 1c shows as-received 10 nm $Mg(OH)_2$ powder and converted MgO powder along with ICSD references. The as-received powder shows only $Mg(OH)_2$ peaks while the converted shows only MgO peaks supporting DSC-TGA data. SEM Micrographs (Fig. 2b) of converted powder reveal very fine grain sizes. The histogram shown in the inset show AGS is 29 nm with a tight distribution (standard deviation of 13 nm). By contrast the commercially available nc-MgO powder (Fig. 2a) has a measured AGS of 42 nm with a broader distribution (22 nm).

In order to study the effect of water content on the densification, the converted 29 nm MgO powder was exposed to ambient environments for 24 h. Some of the converted powder was exposed to a humid environment for varying durations (1—3h), in which ambient air was filtered and passed through a blubber filled with UHP water with flow-controller. To ascertain the absorbed amount of water, the powder was weighed before and after exposure to the environment. The data is reported according to two limiting case conditions: 1) Assuming absorbed water remains H_2O on the MgO surface and 2) Assuming absorbed water reacts with MgO to form $Mg(OH)_2$. The latter is a good assumption since the hydroxylation reaction is thermodynamically favorable ($\Delta G < 0$) at room temperature. The results are tabulated in two columns, wt% H_2O-gained and mol% $Mg(OH)_2$ in Table 1. The results indicate 0–17 wt% H_2O or 0–39 mol% $Mg(OH)_2$. XRD did not suggest the formation of crystalline $(MgOH)_2$ after the exposure.

Interestingly, the XRD profile of the sample densified from 0 wt%–29 nm powder initially showed a different peak intensity-ratio compared to the 42 nm powder and MgO reference, indicating preferential grain alignment (texturing) in the bulk sample (Fig. 1c, No PBM). Planetary ball-milling (PBM) of the 29 nm powder prior to densification in CAPAD resulted in a bulk sample with same peak intensity-ratio as the reference, solving the texturing issue (Fig. 1c, PBM). XRD of densified bulk from powder with the highest water content, 17.2 wt% initial, shows very minor hydroxide peaks indicated by red diamonds. The relatively low intensity of the $Mg(OH)_2$ XRD peaks could be caused by thin layers of $Mg(OH)_2$ remaining in the sample volume after densification. In addition, $Mg(OH)_2$ has a lower crystallinity (is more defected) compared to MgO, causing MgO peaks to be significantly more intense.

Micrographs of fracture surfaces of bulk samples are shown in Fig. 2 (c–d). 29 nm powders densified with or without exposure to humid air were examined. The microstructure is very similar and shows a fine nanocrystalline grain structure. The AGS was measured using the longest distance across a grain for >300 individual grains from each micrograph. The grain size distributions are shown in insets Fig. 2. Interestingly, there was no significant difference in AGS and distribution; The AGS = 51.6 ± 18.1 nm for the 0 wt% and 52.1 ± 21.9 for the 17.2 wt% sample. This in contrast with Anderson and Morgan [9] who observed increased grain growth rates in pressure-less sintering in water vapor. We believe the similar grain sizes are caused by similar diffusion-controlled densification as discussed below.

Fig. 3a shows the RD of the CAPAD densified samples as a function of grain size and wt%H_2O gained. The RD of the sample densified from 42 nm MgO was 93.5% while the sample densified from 29 nm powder was 96%. We attribute the higher density of the latter to increased

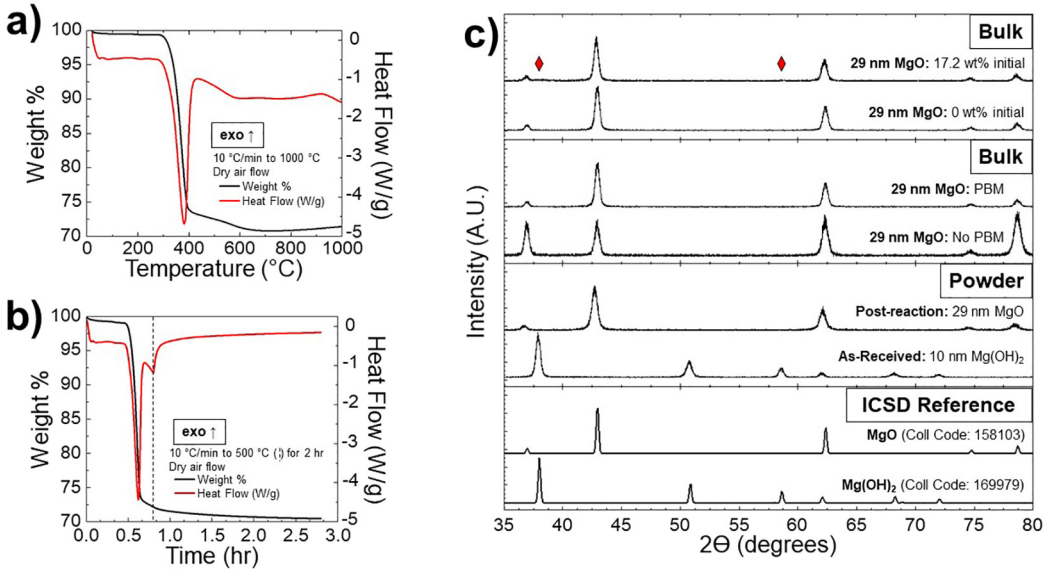

Fig. 1. a) TGA-DSC of as-received 10 nm Mg(OH)2 powder at 10 °C/min to 1000 °C. b) TGA-DSC with parameters to replicate furnace reactions of Mg(OH)2, showing completed reaction after 2 h at 500 °C. c) X-ray diffraction of powders and densified bulk samples. ICSD references are included for comparison.

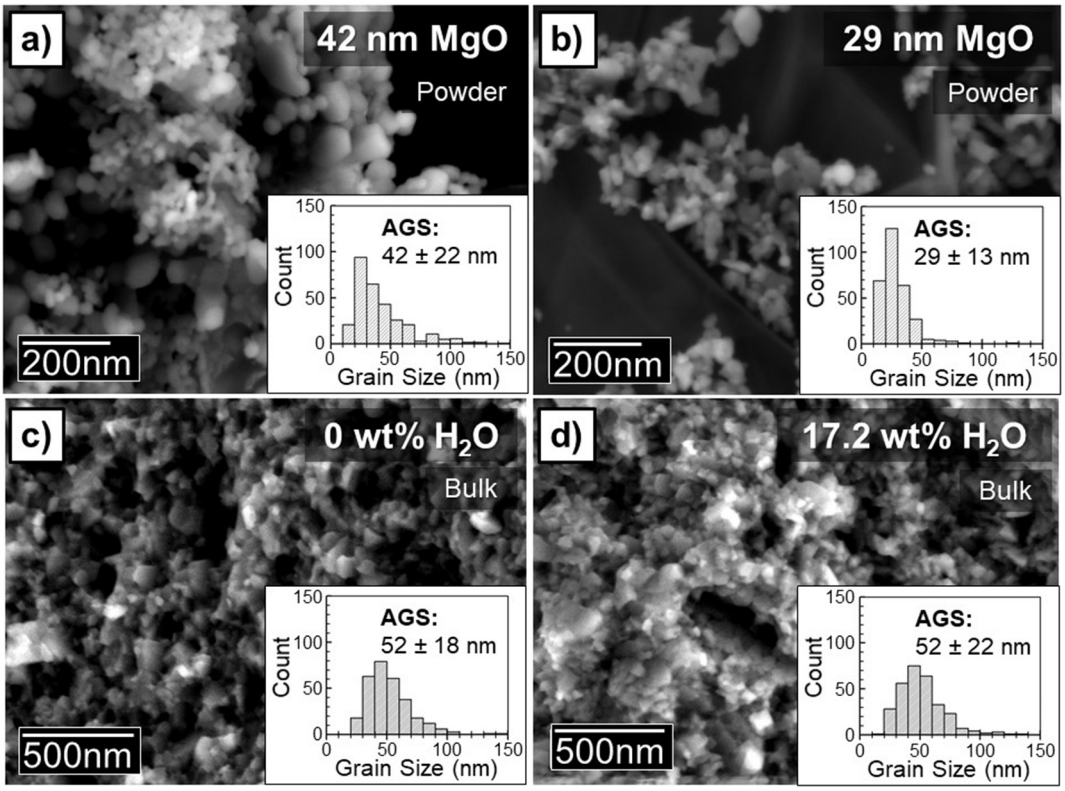

Fig. 2. SEM Micrographs of powder and densified samples a) as-received 42 nm MgO, and b) 29 nm MgO reacted from as-received 10 nm Mg(OH)2. Fractured surfaces of CAPAD produced samples from c) 29 nm MgO with 0 wt% and d)17.2 wt% gained. Insets show the histograms of the AGS.

densification rates caused by finer grain sizes as will be discussed below. Although 96% density is typically interpreted as 4% porosity, we believe that the porosity in the densified samples could be significantly lower. Grain boundary (gb) regions are known to have lower density (more open structure) compared with grain interiors especially in nanocrystalline materials and thus the RD can be lowered even with little/no porosity. In a sample with AGS = 51 nm, a 4% reduction in RD can be caused by an effective grain boundary density of 31% of the MgO theoretical density (assuming gb thickness = 1 nm) which is in-line with calculations and experimental observation of grain boundary structures in MgO [13].

The processing times and temperatures required for densification are in-line with previous CAPAD of nc-MgO. Chaim et al. achieved >98% RD of nc-MgO at 150 MPa and 825 °C for 5 min [4]. TB Tran and coworkers used significantly higher pressures (300–500 MPa) and temperatures ranging from 650 to 800 °C and achieved >99% RD with very fine grain sizes ~25 nm.

The presence of $Mg(OH)_2$ (2.34 g/cm^3, 61% of MgO) in the bulk sample can also contribute to lower RD. Fig. 3b plots the wt% gained by the powder vs. the wt% lost after densification; the dashed line represents same wt% lost = wt% gained. We attribute the weight loss to water leaving the sample as a result of the conversion of MgO from $Mg(OH)_2$ during the densification process. The low wt% samples lost the same wt% as gained, while the higher wt% samples retained some of the gained weight, likely as a hydroxide phase. The conclusion that the weight loss was in the form of water vapor is corroborated by chamber pressure measurements taken during the CAPAD experiments (Fig. 3c). These results show that the 0 wt% samples show virtually no increase in chamber pressure, while the 7–17 wt% samples have a significant pressure rise starting a low temperature ~100 °C and increasing dramatically at ~350 °C corresponding to the $Mg(OH)_2$ to MgO conversion (Fig. 1a). If we assume that the remaining water is $Mg(OH)_2$ after densification (suggested by XRD shown in Fig. 1c, top), the RD of composite MgO-$Mg(OH)_2$ bulk samples can be recalculated and is shown in Table 1. Recalculation suggests all samples exhibit RD > 95%.

A temperature of 700 °C required to densify MgO is surprisingly low given its high melting point. Although electric current/field effects are relevant for CAPAD of materials with relatively high electrical conductivity we do not believe these play a large role in MgO. Instead we believe these low temperatures are in part caused by fine grain sizes of the starting powder <50 nm. Another reason for a low densification temperature is the possible influence of absorbed water and/or hydroxide formation which has been previously shown to influence densification temperatures in MgO and other oxides. We measured densification

Table 1
Summary of 5 samples prepared with varying weight percent of adsorbed species, ordered by wt% adsorbed by powder pre-CAPAD. Wt% calculations are both a function of the initial weight (pre-absorption). Mol% $Mg(OH)_2$ calculations consider all weight gained as contributing to $Mg(OH)_2$ formation.

Powder	wt% H2O gained, pre CAPAD	mol% Mg(OH)2 pre CAPAD	wt% H2O lost, post CAPAD	Bulk R.D. (%)	Composite Bulk R.D. (%)[a]
42 nm MgO	0	0	0.9	93.5	–
	0	0	0.9	96.1	–
29 nm MgO	7.6	17.0	7.7	95.3	–
	10.8	24.2	8.4	93.2	95.7
	17.2	38.5	10.9	92.9	99.5

[a] Assuming all remaining H2O post CAPAD converts to Mg(OH)2.

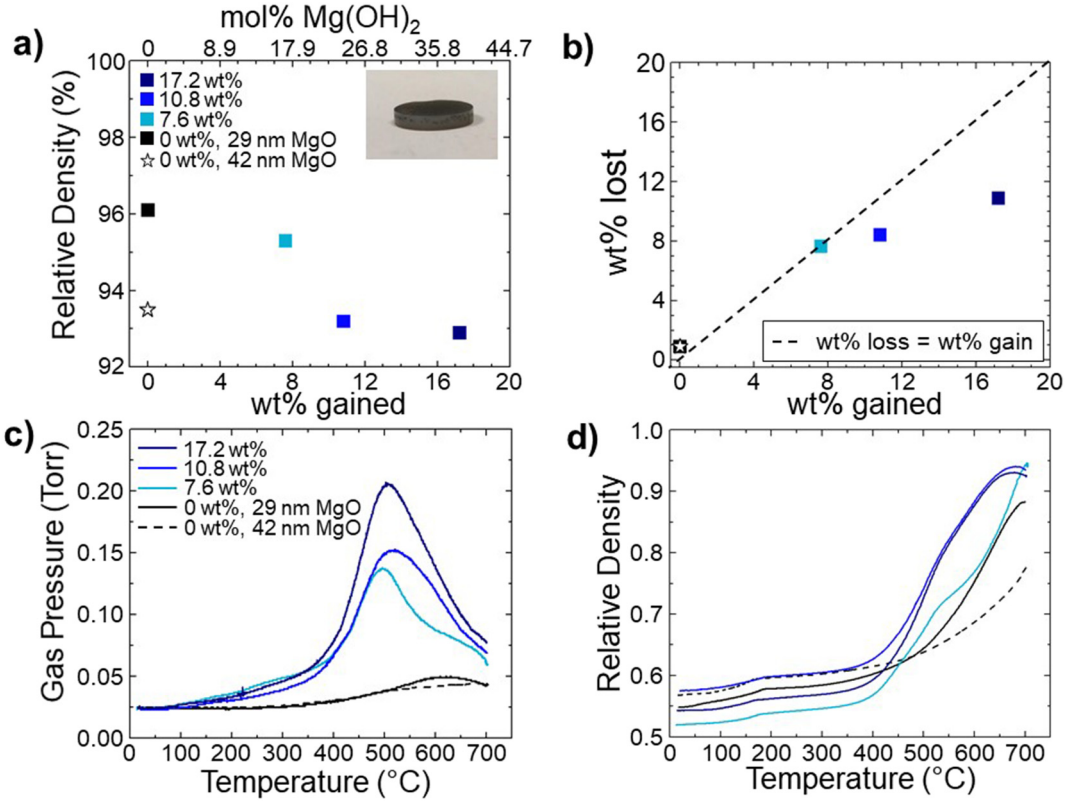

Fig. 3. a) Relative density of CAPAD processed samples as a function of wt% gained of powder pre-CAPAD. The inset shows a picture of a densified sample (0 wt% 29 nm MgO) with 9.5 mm diameter. b) Measured wt% gained of powder before CAPAD vs. sample wt% lost after CAPAD c) CAPAD chamber pressure measured during densification of MgO powders with varying wt% gained and initial grain size c) real-time relative density of samples vs. CAPAD temperature. These curves were corrected for thermal expansion/elastic deformation and weight loss during densification.

as a function of time, $\rho(t)$ using the real time data acquired during CAPAD experiments and the relation:

$$\rho(t) = \frac{m(t)}{V(t)} = \frac{m(t)}{A_c(l_0 - l(t))} \tag{2}$$

where m is mass, V, is the sample volume, A_c is the cross-sectional area, l_o initial height and l is the height change measured during the experiment. Since the A_c of the die is known, and l_o can be measured, the denominator in Eq. (2) depends only on the length contraction during the experiment. The load frame in our CAPAD instrument has a displacement resolution of 0.0747 μm and a load measurement accuracy of 0.4%. As is typically done [14,15], we removed thermal expansion/elastic deformation caused by machine and graphite tooling from $l(t)$ by running blank die experiments with the same temperature profile. The true density as measured using Eq. (2) can be converted to real-time RD, by dividing by theoretical density.

Since 7–17 wt% samples have significant weight loss, we used the chamber pressure (vacuum) data recorded during CAPAD experiments (Fig. 3c) calibrated with measured weight loss (Table 1) to find time dependent mass, $m(t)$. The measured chamber pressure was integrated to obtain total pressure, normalized and converted to mass by multiplying by the measured mass loss. The $m(t)$ data was corrected for time dependent chamber pressure change from system (caused by temperature changes and de-gas from the chamber/tooling) by removing data recorded using a blank die experiment.

The RD as a function of temperature is shown in Fig. 3d. The dry samples (0 wt%) show small amount of continuous densification that significantly increases at ~500 °C. These curves are similar to densification vs. temperature curves calculated for MgO by Reis and Chaim using diffusion-controlled HIP equations proposed by Artz et al [16], modified to include grain growth [17]. Thus, we believe the densification in our "dry" MgO is controlled by diffusional densification mechanisms. By contrast the 7-17 wt% samples have significantly lower onset of densification temperatures ~350 °C.

In order to further investigate possible mechanisms, we found $\dot{\rho}$ by numerically differentiating the $\rho(t)$ curves. The densification rate as a function of temperature, $\dot{\rho}(t)$ for the samples with varying wt% H_2O is shown in Fig. 4a. $\dot{\rho}_{max}$ vs. homologous temperature, T/T_m is plotted in Fig. 4b. The $\dot{\rho}$ of the 0 wt% nc-MgO increases continuously at low T and shows a relatively broad peak at ~600 °C. The curve shapes are similar to $\dot{\rho}$ vs. T we measured previously for nanocrystalline yttrium stabilized ZrO_2 (nc-YSZ) and nc-Si [15]. The magnitude of the maximum densification rate, $\dot{\rho}_{max} = 2.7 \times 10^{-3}\ s^{-1}$ for nc-MgO densified from larger grain size (42 nm) is in the same order of magnitude as that previously measured for nc-YSZ and nc-Si ($\dot{\rho}_{max}$ ~$5 \times 10^{-3}\ s^{-1}$). The grain size of the starting powder of both nc-Si and nc-YSZ was ~50 nm. By contrast, $\dot{\rho}_{max} = 5 \times 10^{-3}\ s^{-1}$ for nc-MgO from finer grain size powder (29 nm) is approximately 2 times higher. We attribute higher $\dot{\rho}$ to the finer grain as suggested in (Eq. (1)).

The $\dot{\rho}$ vs. T curve of the 7.6 wt% H_2O sample shows a dramatically different shape compared with the dry, 0 wt% samples; instead of one broad $\dot{\rho}$ peak, there are now two. The peak in the higher T regime is diffusion-controlled densification as mentioned previously. The $\dot{\rho}_{max}$ occurs in a similar T range as the 0 wt%, but there is an additional peak with similar magnitude located at 500 °C. The two distinct peaks suggest that there are differing controlling densification mechanisms in these regions. In addition, the relative magnitude of these two peaks switch, *i.e* the $\dot{\rho}_{max}$ is now at the lower T/T_m regime for the high H_2O content samples. Interestingly, the curve for higher wt% samples (10.8 wt% and 17.2 wt%) still shows two peaks, but the peaks are more convoluted. This observation implies that continue to be controlling densification

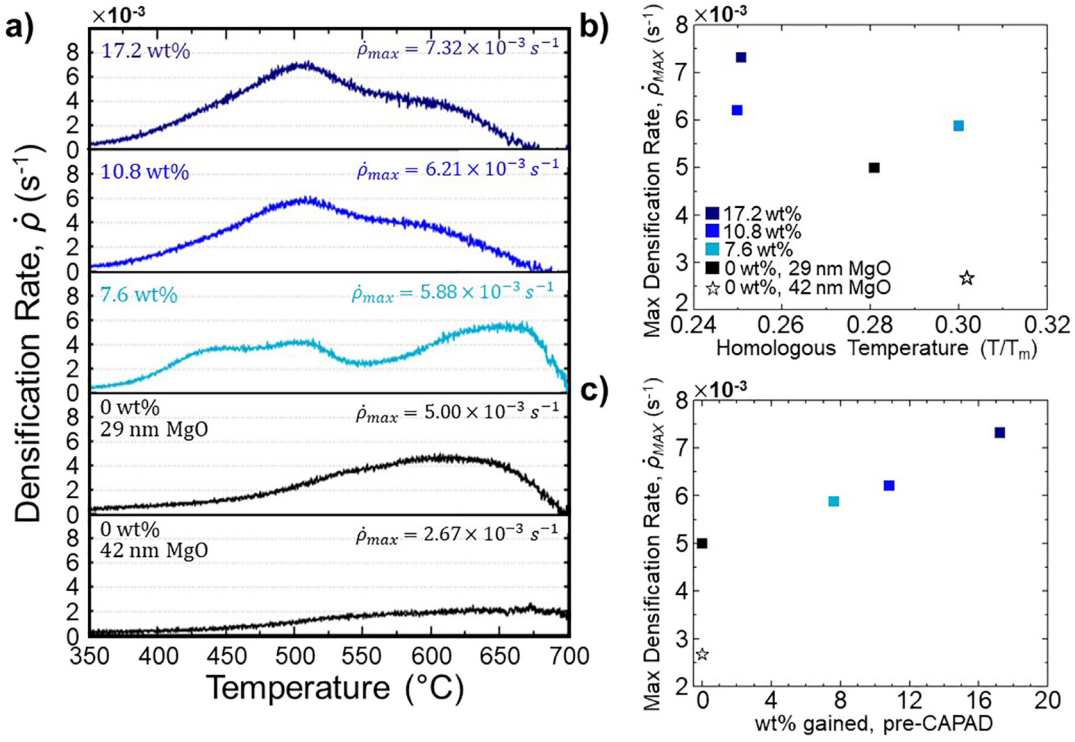

Fig. 4. a) Densification rate for varying grain size and wt% gained of initial powders. The data has been corrected for mass loss during densification. b) maximum densification rate as a function of homologous temperature c) maximum densification rate as a function wt% gained from exposure to H_2O vapor.

mechanisms, but the dominant densification mechanism is different for samples with higher wt%H_2O. Increases in wt% gained increases $\dot{\rho}$ (Fig. 4c), but do not significantly change the location of the peaks, suggesting that the densification mechanism remain the same. We attribute this lowered densification temperature to particle/grain rearrangement caused by $Mg(OH)_2$ to MgO conversion. $Mg(OH)_2$ forms around MgO after exposure to moisture and during densification it converts to MgO resulting in a −54.8% volume change that triggers grain rearrangement aided by the applied pressure. The existence of the diffusion-controlled peak in all the samples explains the similar grain size of the 0 and 17.2 wt% densified samples (Fig. 2).

The densification of nanocrystalline ceramic powders is a well-recognized approach to obtain nanocrystalline bulk samples with properties significantly different from their larger-grained counterparts. In addition to grain size effects, this study demonstrated the lesser known effect of absorbed water/hydroxide on the densification of oxides with >50 nm grain size. Since significant reduction of grain size increases the specific surface area available for absorption and formation of hydroxide, the influence of water/hydroxide on the densification become more significant. We believe the results presented here provide additional insight into the densification of nanocrystalline oxide powders.

Acknowledgments

This work is dedicated to the memory of our dear friend and colleague, Prof. H. W. Green. Funding from the National Science Foundation (NSF EAR-1345130) is gratefully acknowledged. We also thank A. Yazdani for help with DSC measurements.

References

[1] R. Chaim, Z. Shen, M. Nygren, J. Mater. Res. 19 (9) (2004) 2527–2531.
[2] Tien B. Tran, et al., J. Am. Ceram. Soc. 95 (4) (2012) 1185–1188.
[3] Wakahara, Shingo, et al. "Phosphorescent luminescence of pure magnesium oxide transparent ceramics produced by spark plasma sintering." Opt. Mater. 35.3 (2013): 558–562.
[4] Jiang, Nan, et al. "Fabrication of sub-micrometer MgO transparent ceramics by spark plasma sintering." J. Eur. Ceram. Soc. 37.15 (2017): 4947–4953.
[5] A.S. Helle, K.E. Easterling, M.F. Ashby, Acta Metall. 33 (1985) 2163–2174.
[6] R. Suryanarayanan Iyer, S.M.M. Sastry, Acta Mater. 47 (1999) 3079–3098.
[7] David Ehre, Elazar Y. Gutmanas, Rachman Chaim, J. Eur. Ceram. Soc. 25 (16) (2005) 3579–3585.
[8] P. Js Anderson, P.L. Morgan, Trans. Faraday Soc. 60 (1964) 930–937.
[9] J.A. Varela, O.J. Whittemore, J. Am. Ceram. Soc. 66 (1) (1983) 77–82.
[10] Paul F. Eastman, Ivan B. Cutler, J. Am. Ceram. Soc. 49 (10) (1966) 526–530.
[11] J.-P. Maria, X. Kang, R.D. Floyd, E.C. Dickey H. Guo, J. Guo, A. Shuichi Funihashi, Clive A. Randall, J. Mater. Res. 32 (17) (Sep 14, 2017).
[12] J. Nie. Y. Zhang, J. M. Chan, R. Huang and J. Lu "Water-assisted flash sintering: flashing ZnO at room temperature to achieve ~ 98% density in seconds" Scr. Mater. 142 (2018) 79–82.
[13] Y. Yan, M.F. Chisholm, G. Duscher, A. Maiti, S.J. Pennycook, S.T. Pantelides, Phys. Rev. Lett. (1998) 3675.
[14] J.E. Garay, Annu. Rev. Mater. Res. 40 (2010) 445–468.
[15] J.E. Alaniz, et al., Scr. Mater. 92 (2014) 7–10.
[16] E. Artz, Acta Metall. 30 (1982) 1883–1890.
[17] J. Reis, R. Chaim, Mater. Sci. Eng. A 491 (1–2) (2008) 356–363.